

# Pressure-induced superconductivity in $\text{CaC}_2$

Yan-Ling Li<sup>a,b</sup>, Wei Luo<sup>b,c</sup>, Zhi Zeng<sup>d</sup>, Hai-Qing Lin<sup>e</sup>, Ho-kwang Mao<sup>f,g,1</sup>, and Rajeev Ahuja<sup>b,c,1</sup>

<sup>a</sup>School of Physics and Electronic Engineering, Jiangsu Normal University, Xuzhou 221116, People's Republic of China; <sup>b</sup>Condensed Matter Theory Group, Department of Physics and Astronomy, Uppsala University, SE-751 20 Uppsala, Sweden; <sup>c</sup>Applied Material Physics, Department of Materials Science and Engineering, Royal Institute of Technology, SE-100 44 Stockholm, Sweden; <sup>d</sup>Key Laboratory of Materials Physics, Institute of Solid State Physics, Chinese Academy of Sciences, Hefei 230031, People's Republic of China; <sup>e</sup>Beijing Computational Science Research Center, Beijing 100084, People's Republic of China; <sup>f</sup>Geophysical Laboratory, Carnegie Institution of Washington, Washington, DC 20015; and <sup>g</sup>Center for High Pressure Science and Technology Advanced Research, Shanghai 201203, People's Republic of China

Contributed by Ho-kwang Mao, April 23, 2013 (sent for review February 1, 2013)

**Carbon can exist as isolated dumbbell, 1D chain, 2D plane, and 3D network in carbon solids or carbon-based compounds, which attributes to its rich chemical binding way, including  $sp$ -,  $sp^2$ -, and  $sp^3$ -hybridized bonds.  $sp^2$ -hybridizing carbon always captures special attention due to its unique physical and chemical property. Here, using an evolutionary algorithm in conjunction with ab initio method, we found that, under compression, dumbbell carbon in  $\text{CaC}_2$  can be polymerized first into 1D chain and then into ribbon and further into 2D graphite sheet at higher pressure. The  $C2/m$  structure transforms into an orthorhombic  $Cmcm$  phase at 0.5 GPa, followed by another orthorhombic  $Immm$  phase, which is stabilized in a wide pressure range of 15.2–105.8 GPa and then forced into  $\text{MgB}_2$ -type phase with wide range stability up to at least 1 TPa. Strong electron–phonon coupling  $\lambda$  in compressed  $\text{CaC}_2$  is found, in particular for  $Immm$  phase, which has the highest  $\lambda$  value (0.562–0.564) among them, leading to its high superconducting critical temperature  $T_c$  (7.9~9.8 K), which is comparable with the 11.5 K value of  $\text{CaC}_6$ . Our results show that calcium not only can stabilize carbon  $sp^2$  hybridization at a larger range of pressure but also can contribute in superconducting behavior, which would further ignite experimental and theoretical interest in alkaline–earth metal carbides to uncover their peculiar physical properties under extreme conditions.**

high pressure | metallization

**H**igh pressure, as a crucial thermodynamic parameter, has been emerging as a powerful tool to investigate physical and chemical behavior of materials, especially to explore the evolution of planets, and synthesize or design materials with peculiar properties such as superhardness and superconductivity (1–5). Recently, Ca and C, as ordinary elemental solids, have been studied extensively in physical, chemical, and material science fields due to their interesting structural properties when pressure is applied (6–10). These peculiar physical properties of compressed Ca and C solids have motivated our attention on Ca-based dicarbide  $\text{CaC}_2$ . In  $\text{CaC}_2$  (11, 12) at ambient pressure, experimentally, four temperature-induced modifications were reported, which are the well-known tetragonal room temperature modification  $\text{CaC}_2$  I (space group  $I4/mmm$ ,  $Z = 2$ ), two low-temperature monoclinic modifications  $\text{CaC}_2$  II ( $C2/c$ ,  $Z = 4$ ), and  $\text{CaC}_2$  III ( $C2/m$ ,  $Z = 4$ ), and cubic high-temperature modification  $\text{CaC}_2$  IV ( $Fm-3m$ ,  $Z = 4$ ) (12). Theoretically, orthorhombic  $\text{CaC}_2$   $Immm$  ( $Z = 2$ , referred to as  $Immm-1$  below) structure, monoclinic  $\text{CaC}_2$   $C2/m$  ( $Z = 2$ , referred to as  $C2/m-1$  below) structure, and trigonal  $\text{CaC}_2$   $R-3m$  ( $Z = 1$ ) structure, were predicted by Kulkarni et al. (13) using a global exploration method based on simulated annealing scheme. In all structures reported above, carbon atoms form isolated dumbbells. Because both Ca and C solids tend to form C-atom network structures at ambient and high pressure (6–10), it is reasonable and interesting to investigate pressure-induced possibility of polymerization of isolated  $\text{C}_2$  dumbbells in  $\text{CaC}_2$ . To our knowledge, there are few studies on compressed  $\text{CaC}_2$  so far. Kulkarni et al. (13) observed that  $C2/m-1$  structure transforms into  $R-3m$  structure at about

24 GPa using local density approximation or 34 GPa using B3LYP. Srepusharawoot et al. (14) studied pressure-induced carbon network formation for five alkaline–earth metal dicarbides (AEMDs) using ab initio random-searching method. Very recently, structural and vibrational properties of AEMD  $\text{BaC}_2$  at ambient temperature and high pressure up to 40 GPa were reported experimentally (15). Amorphous states were observed, which can be viewed as a precursor for the formation of carbon networks embedded in a metal framework.

Covalent bonding and ionic bonding coexist in AEMDs. There is a strong covalent bonding in  $\text{C}_2$  units, but ionic in between Ca and C. Up to now, there have been many open questions for compressed AEMD: (i) How did  $\text{C}_2$  dumbbell evolve after applying pressure? (ii) Could it be metallized under reasonable pressure? (iii) Is the metallic high-pressure phase a superconductor? Here, we select  $\text{CaC}_2$  as an example to address these problems.

The structural properties of  $\text{CaC}_2$  at high pressure were investigated by using global structural searching scheme based on an evolutionary algorithm (EA) (16, 17) in combination of first-principles total energy calculations. At high pressure, it was found that  $\text{CaC}_2$  adopt the layered structures, in which carbon atoms first form chains and then ribbons or graphene sheets separated by Ca atomic layers. Of the three of the predicted high-pressure phases, two have orthorhombic symmetry ( $Cmcm$  and  $Immm$ ) and the third one is a well-known  $\text{MgB}_2$ -type structure with  $P6/mmm$  symmetry. Calculated vibrational properties are similar to those observed in  $\text{CaC}_6$  (18). The electronic structure calculations show that all of the three predicted high pressure phases are metallic. Finally, phonon-mediated superconducting behavior of three new high-pressure phases of  $\text{CaC}_2$  was revealed by exploring electron–phonon coupling.

Knowledge of the structural information is the first step toward understanding the physical properties of any material. To get the most stable structure of  $\text{CaC}_2$ , we searched for its lower enthalpy's phase based on EA in combined with Vienna ab initio simulation package (VASP) package. We performed variable-cell structure prediction simulations using USPEX code for  $\text{CaC}_2$  containing two, three, and four molecules in the simulation cell at 5, 20, 40, 80, 120, 200, 300, 500, and 700 GPa, and 1 TPa, respectively. During the evaluation, the total energy was calculated via the VASP package. For comparison, the structures discussed in  $\text{BeC}_2$ ,  $\text{MgC}_2$ , and  $\text{BaC}_2$  experimentally and theoretically, are also considered in our calculations. The enthalpies per chemical formula unit vs. pressure curves of selected structures are plotted in Fig. 1. Considering that  $I4/mmm$ ,  $C2/m$ ,  $C2/c$ ,  $C2/m-1$ , and  $Immm-1$  structures hold very close enthalpy, their

Author contributions: Y.-L.L. and R.A. designed research; Y.-L.L. performed research; Y.-L.L., W.L., Z.Z., H.-Q.L., H.-k.M., and R.A. analyzed data; and Y.-L.L., W.L., and R.A. wrote the paper.

The authors declare no conflict of interest.

<sup>1</sup>To whom correspondence may be addressed. E-mail: rajeev.ahuja@physics.uu.se or mao@gl.ciw.edu.

This article contains supporting information online at [www.pnas.org/lookup/suppl/doi:10.1073/pnas.1307384110/-DCSupplemental](http://www.pnas.org/lookup/suppl/doi:10.1073/pnas.1307384110/-DCSupplemental).

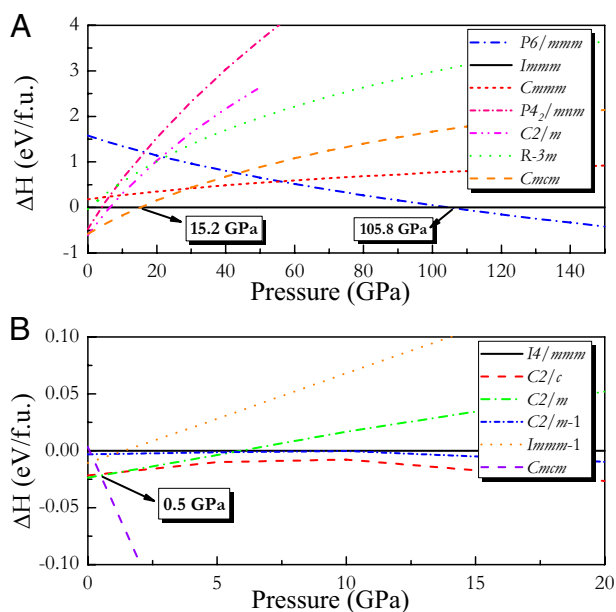


**Fig. 1.** The relative enthalpy per chemical formula molecule as a function of pressure for competing structures. The phase transition series monoclinic  $C2/m$  phase to orthorhombic  $Cmcm$  phase (0.5 GPa) to another orthorhombic  $Immm$  phase (15.2 GPa) to hexagonal  $P6/mmm$  phase (105.8 GPa) obtained. Further calculations determined the stability of hexagonal phase up to 1 TPa.

enthalpies vs. pressure curves are specially given in Fig. 1B, in which  $I4/mmm$ ,  $C2/c$ , and  $C2/m$  refer to three modifications determined at different temperature by experiments, whereas  $C2/m-1$  and  $Immm-1$  represent lower enthalpy structures suggested by a global exploration method based on simulated annealing (13). From Fig. 1, one can see that, for compressed  $\text{CaC}_2$ , the monoclinic  $C2/m$  structure (referred as phase I) is the most stable structure below 0.5 GPa. An orthorhombic  $Cmcm$  phase (referred as phase II) takes over the pressure range from 0.5 to 15.2 GPa. Another orthorhombic  $Immm$  structure (referred to as phase III) is the most stable structure over the wide pressure range of 15.2–105.8 GPa, followed by a  $\text{MgB}_2$ -type structure (space group  $P6/mmm$ , referred to as phase IV) at 105.8 GPa above. Among these, phases II, III, and IV are metallic. Our total energy calculations rule out other competitive low-enthalpy structures that exist in  $\text{MgC}_2$ ,  $\text{CaC}_2$ , and  $\text{BaC}_2$ , including  $I4_1/amd$  (16),  $P4_2/mnm$  (19),  $P4_332$  (20),  $I4/mmm$ ,  $C2/m-1$ ,  $Immm-1$ ,  $P6_3/mmc$ , and  $R-3m$  (13). Our calculations show that the previous  $R-3m$  structure of  $\text{CaC}_2$  suggested theoretically (13) is not a favorable one (Fig. 1). In addition,  $Cmmm$  structure, a metastable phase, has comparative enthalpy with phases III and IV at large pressure range due to their similar structural properties (atomic layered arrangement). The optimized structural parameters at different pressure are listed in Table S1. For phase II, the equilibrium lattice constants at 4 GPa are  $a = 3.6822 \text{ \AA}$ ,  $b = 8.6324 \text{ \AA}$ , and  $c = 4.7360 \text{ \AA}$ . In this structure, four calcium atoms lie in the Wyckoff  $4c$  site and eight carbon atoms occupy the  $8f$  site, in which calcium atoms construct cylinder with hexagon cross-section, centered by one-dimensional (1D) arm-chair carbon chain along  $z$  direction (Fig. 2C). The equilibrium lattice constants of phase III at 15.2 GPa are  $a = 7.0623 \text{ \AA}$ ,  $b = 2.6317 \text{ \AA}$ , and  $c = 6.2697 \text{ \AA}$ . Four calcium atoms hold the Wyckoff  $4e$  sites and eight C atoms occupy two inequivalent Wyckoff  $4i$  (referred as C1) and  $4j$  (referred as C2) sites. It is worthwhile to note that phase III suggested here differs clearly from the  $Immm-1$  phase predicted by simulated annealing (13). The  $Immm-1$  phase includes two molecules per unit cell, in

which carbon atoms form isolated dumbbells, whereas our stable phase III contains four molecules per unit cell, in which carbon atoms were polymerized into nanoribbon with a six-membered ring. From Fig. 2D, one can see that a carbon nanoribbon, forming quasi-1D carbon ribbons, lies in the center of cylinder constructed by calcium atoms. For phase IV, a  $\text{MgB}_2$ -type structure, including only one molecule per unit cell, the equilibrium lattice parameters at 105.8 GPa are  $a = 2.5412 \text{ \AA}$  and  $c = 3.6864 \text{ \AA}$ . One calcium atom exists in  $1a$  site and two carbon atoms lie in  $2d$  sites. Structurally, phase IV of  $\text{CaC}_2$  consists of hexagonal honeycombed layers (referred as graphene sheet) of carbon atoms separated by planes of Ca atoms, with the calcium atoms centered above and below the carbon hexagons (Fig. 2B). Also, we have noticed that pressure-induced phase transition in  $\text{CaC}_2$  is first-order phase transition because of an obvious change in volume at the phase transition point. Under chemical pre-compression and external compression, dumbbell-type carbon is

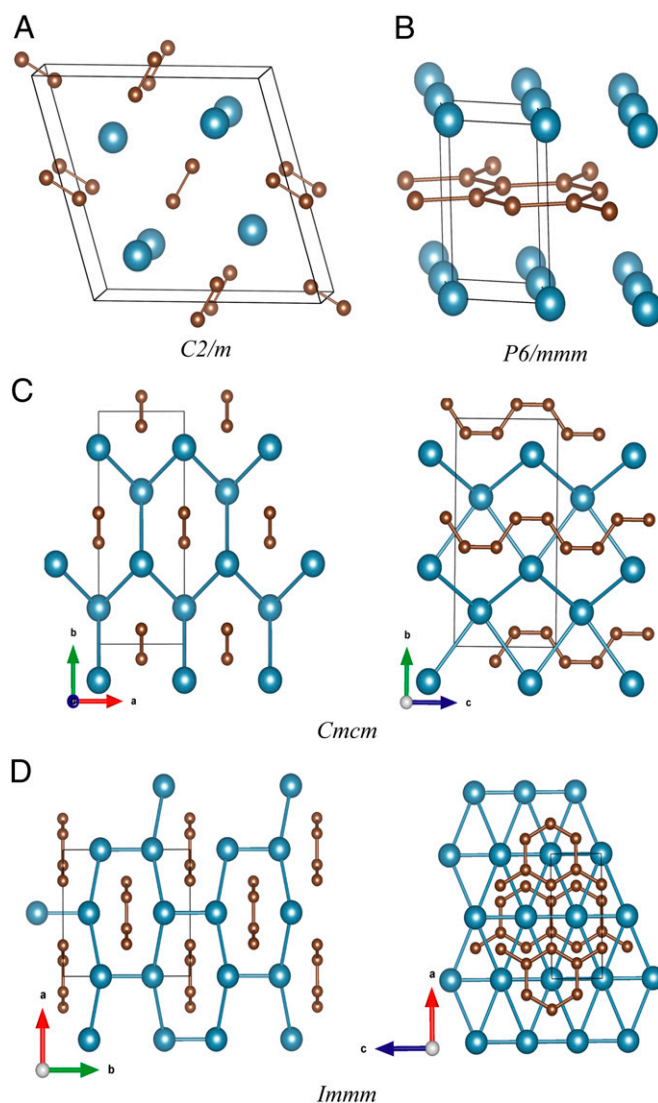


**Fig. 2.** Phase  $C2/m$  and three new phases of  $\text{CaC}_2$ . The big and small balls represent calcium and carbon atoms, respectively. One-dimensional armchair carbon chains along  $c$ -axis direction observed in  $Cmcm$ . One-dimensional carbon ribbons and 2D graphene sheets observed in  $Immm$  and  $P6/mmm$  phases, respectively. In  $Immm$ , calcium atoms construct cylinder with hexagon cross-section, which is arranged periodically, centered by 1D carbon ribbon (Left of D).

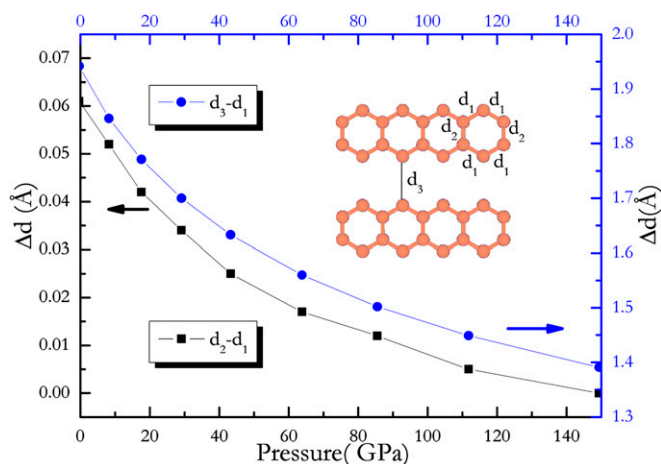


**Fig. 3.** Change of structural property for ribbon formed by carbon atoms in *Immm* phase with increasing pressure. Upon compression, the lengths of two kinds of C–C bonds in ribbon tend to be uniform.

polymerized first into ordered armchair chain and further into quasi-1D well-ordered nanoribbon and eventually into 2D graphite sheets (graphene). Besides this, we did explore possibility of 3D network carbon under higher pressure until 1 TPa based on EA. Surprisingly, all performed calculations always point to a  $MgB_2$ -type (*P6/mmm*) structure. Phonon calculation further confirms its dynamical stability.

It will be constructive to look at the change of carbon–carbon bonding with increasing pressure to study the structural phase transformation mechanism. From low-pressure phase to high-pressure phase, C–C bonding behavior reveals obvious change due to external pressure and internal chemical precompression. Applying pressure to  $CaC_2$ , *I4/mmm* structure with isolated dumbbell space orientation along the *z* axis, which is stable at room temperature observed experimentally, is not energetically favorable compared with those (such as *C2/m*, *C2/c*, *C2m-1*, and *Immm-1*; Fig. 1) that possess isolated dumbbell space orientation keeping an angle with *z* axis. With increasing pressure, the distance between isolated dumbbell decreases, resulting in carbon atomic chain formed at lower pressure (see *Cmcm* structure). Upon further pressure, carbon atomic chain tends to well-organized arrangement, making orthorhombic phase II being transformed into an orthorhombic phase III. In phase III, there are two different bonding lengths (referred as  $d_1$  and  $d_2$ ) in ribbon with six-membered carbon ring (Fig. 3). At the pressure of 10 GPa, two among the six C–C bondings ( $d_1$ ) hold a length of 1.4747 Å, and four of them ( $d_2$ ) have a length of 1.5246 Å. Under further compression, the difference ( $\Delta d$ ) between  $d_1$  and  $d_2$  begins to decrease smoothly (Fig. 3). At the same time, the distance ( $d_3$ ) between neighbor ribbons begins to decrease (Fig. 3). In other words, for phase III, the difference of carbon–carbon bond length gradually decreases with increasing pressure until it disappears at 150 GPa, which results in a formation of a regular hexagonal ring. This kind of pressure-induced structural modification indicates the feasibility of graphite sheet (i.e., graphene sheet) formed in compressed  $CaC_2$ , as is observed in phase IV.

Due to the occurrence of graphite sheet between neighbor Ca atomic layers, phase IV could be one of graphite intercalation compounds (GICs). The properties of the GIC family have been studied extensively using a variety of different experimental techniques (21–25). Especially, the discovery of superconductivity in  $CaC_6$  at the enhanced transition temperature (11.5 K) (26, 27) excited intense research interest in GICs experimentally (28, 29). The C–C bond length in phase IV is 1.4672 Å at 105.8 GPa, which is slightly longer than that (1.42 Å) in graphite. Also, we can see that phase III has a similar structural property as  $CaC_6$  (all of the calcium atoms lie above and below of the center of carbon six-membered ring). This peculiar structural behavior indicates that compressed  $CaC_2$  would present similar physical properties as  $CaC_6$ , such as superconductivity.

It is essential to check mechanical and dynamical stability of low enthalpy phases by means of elastic constants and phonon spectrum. There are 13, 9, and 5 independent elastic constants for monoclinic, orthorhombic, and hexagonal structures, respectively. The calculated elastic constants for four low enthalpy phases of  $CaC_2$  are presented in Table 1. For hexagonal symmetry,  $c_{66}$  is equal to  $(c_{11} - c_{12})/2$ . From Table 1, it is obvious that elastic constants satisfy mechanical stable criterion, implying their stability mechanically. Additionally, bulk modulus *B*, shear modulus *G*, and Young's modulus *E* were obtained using Voigt's formulas. For phase I, the calculated *B*, *G*, and *E* are 55, 24, and 63 GPa. Small *B* value indicates its strong compressibility. We have noticed that volume collapse 19.3% at phase transition point from phase I to phase II. Strong compressibility attributes to highly ionic bonding in between calcium and carbon. For hexagonal phase IV, high elastic moduli originate from strong covalent bonding between carbon atoms.

Phonon calculations show that phases II, III, and IV are stable dynamically at their stable pressure ranges. Phonon dispersions and partial phonon density of states (PPHDOS) of phases II, III, and IV are shown in Fig. 4. The maximum optical branch frequencies are 1,390.4  $cm^{-1}$  for phase II at 1 GPa, 1,129.7  $cm^{-1}$  for phase III at 15.2 GPa, and 1,443.9  $cm^{-1}$  for phase IV at 105.8 GPa, which are lower than the value 1,860  $cm^{-1}$  (30) of room temperature phase *I4/mmm* due to an obvious structural difference. From PPHDOS, one can conclude that calcium atom dominates the low-frequency region, whereas carbon atoms contribute to the high-frequency region. In Fig. 4, flat bands along peculiar direction in Brillouin zone (BZ) indicate layered structural property for three new phases. For phase II, the phonon dispersions possess two frequency gaps (48.4 and 171.6  $cm^{-1}$ , see Fig. 4A), which originate from the stiffening of the carbon chains.

Phase IV contains interesting graphene sheets, so we only discuss its phonon behavior in the following. For phase IV, PPHDOS calculation shows that the Ca-related phonons occur at the lower frequencies typically below 491  $cm^{-1}$  because the Ca atoms are much heavier and more weakly bonded than the C atoms (Fig. 4). In detail, for phase IV,  $Ca_y$  modes mainly occupy in below 400.3  $cm^{-1}$ , whereas  $Ca_x$  and  $Ca_z$  modes dominate the spectrum range from 400.3 to 700.6  $cm^{-1}$ . The graphene sheets in phase IV have strong planer bonding, indicating that the out-of-plane  $C_z$  modes fall between 300.2 and 667.2  $cm^{-1}$ , whereas the in-plane  $C_{xy}$  modes are mainly in higher frequency and dominate the frequencies above 700.6  $cm^{-1}$  (Fig. 4C). So there is

**Table 1.** Independent elastic constants, bulk, shear, and Young's moduli (all in GPa) of stable phases of  $CaC_2$

Space group	P	$c_{11}$	$c_{22}$	$c_{33}$	$c_{44}$	$c_{55}$	$c_{66}$	$c_{12}$	$c_{13}$	$c_{23}$	$c_{15}$	$c_{25}$	$c_{35}$	$c_{46}$	<i>B</i>	<i>G</i>	<i>E</i>
<i>C2/m</i>	0	86	98	91	13	47	6	29	58	22	7	9	−21	5	55	24	63
<i>Cmcm</i>	4	158	188	317	70	72	48	43	68	78					115	70	174
<i>Immm</i>	15.2	338	650	397	162	79	86	64	59	71					197	145	349
<i>P6/mmm</i>	105.8	1,056		824	373		458	141	238						463	396	924

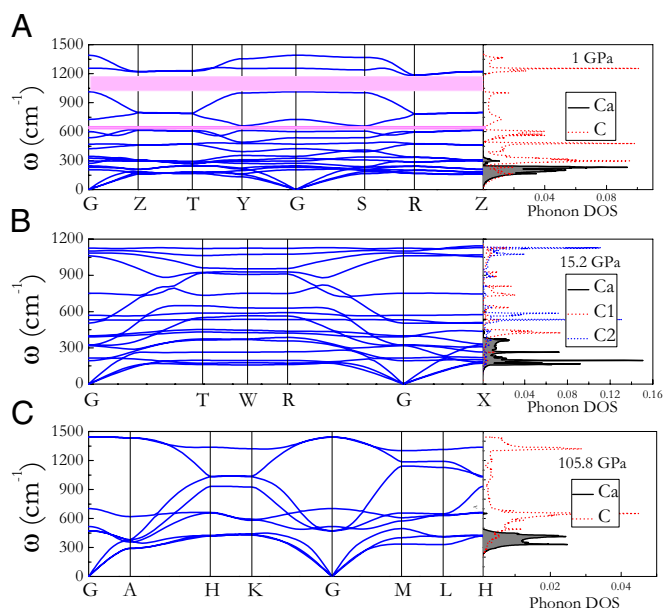


**Fig. 4.** Phonon spectrum and partial atomic phonon density of states of three new phases for cold compressed  $\text{CaC}_2$ . Soft phonon modes are observed in them, in particular, for  $Immm$  phase.

strong coupling between  $\text{Ca}_{yz}$  phonons and  $\text{C}_z$  phonons. The observed carbon atomic vibration behavior here has been determined in well-known Ca-based carbide  $\text{CaC}_6$  experimentally. The most important issue is that the calculated phonon frequency windows of  $\text{C}_z$  modes and  $\text{C}_{xy}$  modes in  $\text{CaC}_2$  are very similar to that observed in  $\text{CaC}_6$ , implying that phase IV of  $\text{CaC}_2$  has similar phonon-related property as  $\text{CaC}_6$ . The partial atomic phonon distribution of phase III is similar to that of phase IV. All three phases possess soft phonon modes at peculiar high-symmetry point direction in BZ. In particular, phase III has more soft modes at the low-frequency region along the G-R, G-X, and G-T directions in BZ (Fig. 4B), which serves as evidence of strong electron-phonon coupling in phase III (discussed below).

Electronic structure calculations show that phase I is a semiconductor (Fig. S1), whereas phases II, III, and IV are metallic. From projected density of states (PDOS) given in Fig. 5, one can see that three metallic phases have consistent electronic distributions.  $\text{C-p}$  electrons dominate in the wide energy range of covalence bands and strongly hybridize with  $\text{Ca-d}$  electrons near the Fermi level (i.e.,  $\text{Ca-d}$  electrons and  $\text{C-p}$  electrons dominate Fermi level). However, there are few  $\text{C-s}$  electrons and  $\text{Ca-s}$  electrons near the Fermi level, denoting a pressure-driven charge transfer from  $s$  electrons to  $p$  or  $d$  electrons, which is confirmed by the atomic Mulliken population analysis shown in Table S2. According to this, one can conclude that the majority of  $\text{Ca-4s}$  electrons transform to  $\text{Ca-d}$  orbital, while the remaining, into  $\text{C}$  atom. For  $\text{C}$  atom, charge transfer is clearly from  $2s$  orbital to  $2p$  orbitals. The pressure-driven  $s-d$  charge transfer makes newly predicted phases being favorable ones energetically. In addition, we considered pressure effect by taking phase III as an example. From Fig. S2, it is obvious that pressure broaden the bands, making conduction band shift to higher level and covalence band shift to lower level. Additionally, PDOS calculations show that, near the Fermi level, the hybridization between  $\text{C-p}$  states and  $\text{Ca-d}$  states is enhanced with increasing pressure.

Observed soft phonon modes, similar vibrational properties as  $\text{CaC}_6$ , and flat energy bands near Fermi level in phase III arouse our interest to explore its superconducting behavior. The calculated spectral function  $\alpha^2F(\omega)$  and integrated  $\lambda(\omega)$  of phases III and IV of  $\text{CaC}_2$  at different pressure were plotted in Fig. 6

(for the case of phase II, see Fig. S3). For phase III, at 17 GPa, the vibrations below  $587.2 \text{ cm}^{-1}$  provide the major contribution to  $\lambda$ , accounting for 66.7% of total  $\lambda$  value (about 0.565). The phonons below  $150.1 \text{ cm}^{-1}$ , which are mostly attributed to the  $\text{Ca}$  atom, contribute only 2.9% of total  $\lambda$  value. The phonons between  $150.1$  and  $280.2 \text{ cm}^{-1}$ , which originates mostly from  $\text{Ca-yz}$  modes (along  $\text{Ca-C1}$  bonding direction) as well as a small quantity of  $\text{C1-yz}$  modes (along  $\text{Ca-C1}$  bonding direction), contribute 39.6% of the total  $\lambda$ . The phonons between  $280.2$  and  $383.6 \text{ cm}^{-1}$ , which originates mostly from  $\text{Ca-x}$  modes (parallel to carbon ribbon plane) as well as a small quantity of  $\text{C1-yz}$  modes (along  $\text{Ca-C1}$  bonding direction), contribute 10.1% of the total  $\lambda$ . The phonons between  $383.6$  and  $587.2 \text{ cm}^{-1}$ , which originates mostly from  $\text{C2-yz}$  modes (along  $\text{Ca-C2}$  bonding direction), contribute 8.7% of the total  $\lambda$ . To summarize, strong electron-phonon coupling, which is necessary for superconductivity in phase III of compressed  $\text{CaC}_2$ , is due to the phonons from  $\text{Ca}$  and  $\text{C1}$  atoms together with electrons from the  $\text{Ca-d}$  and  $\text{C-p}$  states. From Fig. 6, one can see that there is obvious difference between phase III and phase IV in mechanism of electron-phonon coupling. For phase IV, at 105.8 GPa, the vibrations below  $700.6 \text{ cm}^{-1}$  provide the major contribution to  $\lambda$  (about 0.47). The low-frequency phonons (below  $300.2 \text{ cm}^{-1}$ ), which mostly involve the  $\text{Ca}$  atoms yield only 6.6% of total  $\lambda$  value. The phonons between  $300.2$  and  $700.6 \text{ cm}^{-1}$  contribute 75.4% of the total  $\lambda$ . The frequencies at  $700.6 \text{ cm}^{-1}$  above, that is, the in-plane vibration modes from carbon atoms, only contribute 18% of the total  $\lambda$ . These results combined with PPHDOS indicate that out-of-plane  $\text{C}_z$  modes in phase IV dominate superconductivity in phase IV of  $\text{CaC}_2$ , due to the prominent contributions to the electron-phonon interaction. Phonons from out-of-plane  $\text{C}_z$  modes together with the electrons from the  $\text{Ca-d}$  and  $\text{C-p}$  states provide the strong electron-phonon coupling necessary for superconductivity in phase IV of compressed  $\text{CaC}_2$ . Most interesting is that phase IV can dominate wide pressure range (see Figs. S4–S6).

The Allen and Dynes modified equation (31) was used to estimate the superconducting transition temperature  $T_c$  from the value of  $\lambda$  determined above. Taking a typical value of 0.115 for the effective Coulomb repulsion parameter  $\mu^*$ , [which is thought to be able to get  $T_c$  in agreement with 11.5 K (26, 27) of

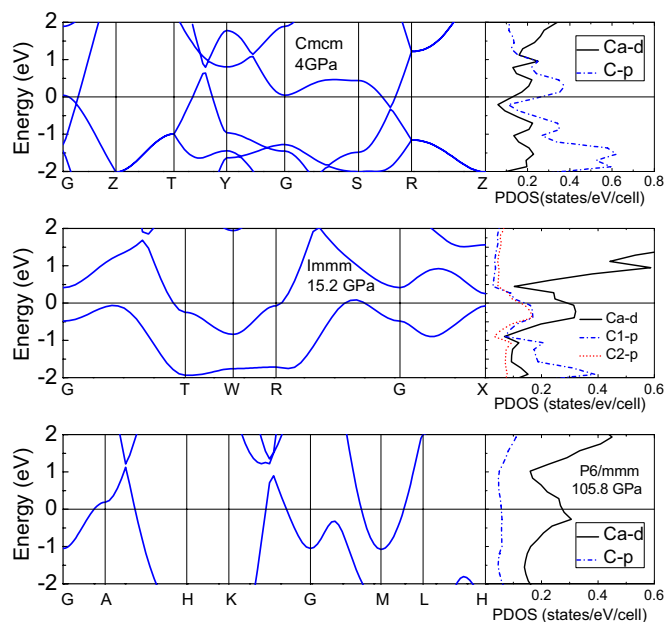


**Fig. 5.** Energy band and projected density of states (PDOS) of  $\text{Cmcm}$  at 4 GPa,  $\text{Immm}$  at 15.2 GPa, and  $\text{P6/mmm}$  at 105.8 GPa. The Fermi level was taken as the energetic reference point.

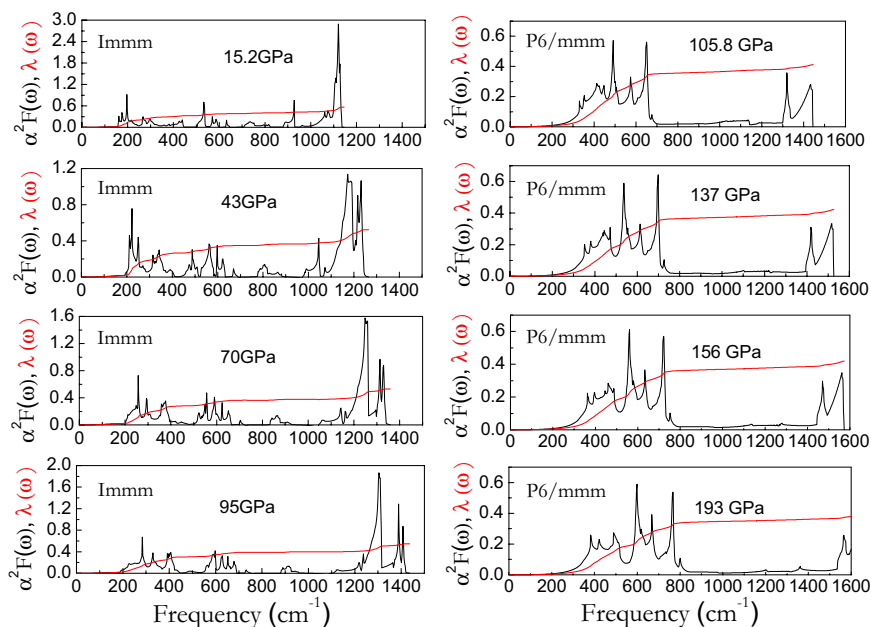


Fig. 6. The Eliashberg phonon spectral function  $\alpha^2 F(\omega)$  (blank line) and integrated  $\lambda(\omega)$  (red line) for *Immm* and *P6/mmm* at four pressure points.

experiment in CaC<sub>6</sub> (32)], we calculated  $T_c$  of three phases for CaC<sub>2</sub> and  $T_c$ 's dependence on pressure. Calculated  $T_c$  values and logarithmic phonon momentum  $\omega_{\log}$  vs. pressure curves are presented in Fig. 7. Logarithmic phonon momentum  $\omega_{\log}$  increases with pressure increase. Among three phases, phase III has the strongest electron–phonon coupling (0.564; Fig. 7, *Inset*) and so have the highest  $T_c$ . At wide range of pressure, phase III of CaC<sub>2</sub> has comparative superconducting critical temperatures (from 7.9 K at 43 GPa to 9.8 K at 95 GPa) with 11.5 K value (26, 27) of CaC<sub>6</sub>.

The structural, dynamical, and electronic properties of compressed CaC<sub>2</sub> were systematically investigated up to 1 TPa. Three stable high-pressure phases, *Cmcm* (phase II), *Immm* (phase III), and MgB<sub>2</sub>-type (phase IV) structures, were predicted by using ab initio EA. The carbon atomic arrangement form from “isolated” dumbbell to 1D chain to quasi-1D ribbon to 2D plane is observed. Phonon calculations have shown their dynamical stability at the dominating pressure range. Strong electron–phonon coupling between Ca-*d* and C-*p* electrons and Ca-*yz* and

C1-*yz* phonons (vibration along Ca-C1 bonding direction) dominates superconductivity of phase III, whereas strong electron–phonon coupling between Ca-*d* electrons and carbon out-of-plane phonons is responsible for superconductivity of phase IV. The predicted evolution of carbon from “local” dumbbell to 2D graphene sheet and high superconducting critical temperature in compressed CaC<sub>2</sub> would stimulate further experimental and theoretical studies on alkaline–earth metal carbides.

## Methods

Ab initio EA, designed to search for the structure possessing the lowest free energy at given pressure and temperature conditions, has been used, using USPEX code (16, 17). The structural and electronic properties of CaC<sub>2</sub> over a wide range of the pressure were performed using density functional theory as implemented in VASP (33), using the projected augmented wave (PAW) pseudopotential included in the released pseudopotential library (34, 35) where  $2s^2 2p^2$  and  $3s^2 3p^6 4s^2$  are treated as valence electrons for C and Ca atoms, respectively. Under the PAW approach, Perdew, Burke, and Ernzerhof's exchange correlation functional (36) was chosen for both Ca and C. For the C atom, we select hard pseudopotential to carry out our calculations because hard pseudopotential was thought to be more suitable for high pressure research. When searching the stable structures, we performed calculations with relaxation of cell volume, cell shape, and ionic positions. Forces on the ions were calculated through derivatives of the free energy with respect to the atomic positions, including the Harris–Foulkes-like correction. All possible structures were optimized using conjugate gradient scheme. For the searches, we used a plane-wave basis set cutoff of 700 eV and performed the Brillouin zone integrations using a coarse k-point grid. The most interesting structures were further relaxed at a higher level of accuracy with a basis set cutoff of 1,000 eV and a k-point grid of spacing  $2\pi \times 0.018 \text{ \AA}^{-1}$ . Iterative relaxation of atomic positions was stopped when all forces were smaller than 0.001 eV/Å.

The dynamical and superconducting properties were calculated in terms of the Quantum Espresso package (37) using Vanderbilt-type ultrasoft pseudopotentials (38) with cutoff energies of 50 and 500 Ry for the wave functions and the charge density, respectively. The electronic BZ integration in the phonon calculation was based on a  $15 \times 15 \times 12$ ,  $15 \times 15 \times 15$ , and  $32 \times 32 \times 24$  of Monkhorst–Pack k-point meshes for phases II, III, and IV, respectively. The electron–phonon coupling was convergent with a finer grid of  $64 \times 64 \times 64$  k points and a Gaussian smearing of 0.01 Ry. The dynamic matrix was computed based on a  $4 \times 4 \times 4$  mesh of phonon wave vectors for phases II and IV and on a  $3 \times 3 \times 3$  mesh of phonon wave vectors for phase III. All calculations were carried out using a primitive cell, which can largely reduce the amounts of computation in comparison with using a unit cell.

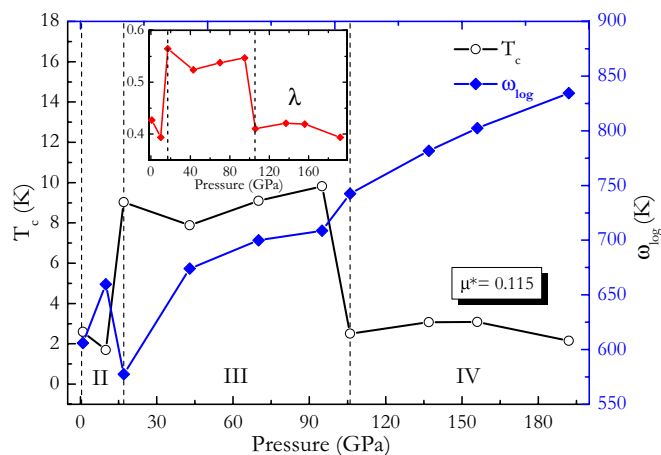


Fig. 7. Calculated  $T_c$  values and logarithmic phonon momentum  $\omega_{\log}$  vs. pressure. *Inset* shows the integrated electron–phonon coupling  $\lambda$  as a function of pressure.

**ACKNOWLEDGMENTS.** This work was supported by National Natural Science Foundation of China Grant 11047013, the Priority Academic Program Development of Jiangsu Higher Education Institutions, and Jiangsu Overseas Research and Training Program for University Prominent Young and Middle-Aged Teachers and Presidents. Part of the calculations was performed at the Center for Computational Science of Hefei Institutes of Physical Science of Chinese Academy of Sciences, the ScGrid of Supercomputing Center and

Computer Network Information Center of the Chinese Academy of Science, and at the Swedish National Infrastructure for Computing. We also thank Swedish Research Council for financial support. H.-k.M. was supported as part of EFree, an Energy Frontier Research Center funded by the Department of Energy, Office of Science, Office of Basic Energy Sciences, under Award DE-SC0001057. Physics and Astronomy Classification Scheme number(s) are as follows: 61.50.Ks, 63.20.D-, 63.20.dk, 63.22.Np, 71.15.Mb.

1. Gillan MJ, Alfe D, Brodholt J, Vocadlo L, Price GD (2006) First-principles modelling of Earth and planetary materials at high pressures and temperatures. *Rep Prog Phys* 69(8):2365–2441.
2. McMillan PF (2006) Chemistry at high pressure. *Chem Soc Rev* 35(10):855–857.
3. Katrusiak A (2008) High-pressure crystallography. *Acta Crystallogr A* 64(Pt 1):135–148.
4. Haines J, Léger J, Bocquillon G (2001) Synthesis and design of superhard materials. *Annu Rev Mater Res* 31(1):1–23.
5. Solozhenko VL, Kurakevych OO, Andrault D, Le Godec Y, Mezouar M (2009) Ultimate metastable solubility of boron in diamond: Synthesis of superhard diamondlike BC<sub>5</sub>. *Phys Rev Lett* 102(1):015506.
6. Knudson MD, Desjarlais MP, Dolan DH (2008) Shock-wave exploration of the high-pressure phases of carbon. *Science* 322(5909):1822–1825.
7. Martinez-Canales M, Pickard CJ, Needs RJ (2012) Thermodynamically stable phases of carbon at multiterapascal pressures. *Phys Rev Lett* 108(4):045704.
8. Nakamoto Y, et al. (2010) Ca-VI: A high-pressure phase of calcium above 158 GPa. *Phys Rev B* 81(14):140106.
9. Sakata M, Nakamoto Y, Shimizu K, Matsuoka T, Ohishi Y (2011) Superconducting state of Ca-VII below a critical temperature of 29 K at a pressure of 216 GPa. *Phys Rev B* 83(22):220512.
10. Tse JS, Desgreniers S, Ohishi Y, Matsuoka T (2012) Large amplitude fluxional behaviour of elemental calcium under high pressure. *Sci Rep* 2:372.
11. Atoji M (1961) Neutron diffraction studies of CaC<sub>2</sub>, YC<sub>2</sub>, LaC<sub>2</sub>, CeC<sub>2</sub>, TbC<sub>2</sub>, YbC<sub>2</sub>, LuC<sub>2</sub>, and UC<sub>2</sub>. *J Chem Phys* 35(6):1950–1960.
12. Knapp M, Ruschewitz U (2001) Structural phase transitions in CaC<sub>2</sub>. *Chemistry* 7(4): 874–880.
13. Kulkarni A, Doll K, Schön JC, Jansen M (2010) Global exploration of the enthalpy landscape of calcium carbide. *J Phys Chem B* 114(47):15573–15581.
14. Srepusharawoot P, Blomqvist A, Araújo CM, Scheicher RH, Ahuja R (2010) One-dimensional polymeric carbon structure based on five-membered rings in alkaline earth metal dicarbides BeC<sub>2</sub> and MgC<sub>2</sub>. *Phys Rev B* 82(12):125439.
15. Efthimiopoulos I, et al. (2012) Structural transformation and vibrational properties of BaC<sub>2</sub> at high pressure. *Phys Rev B* 85(5):054105.
16. Oganov AR, Glass CW (2006) Crystal structure prediction using ab initio evolutionary techniques: Principles and applications. *J Chem Phys* 124(24):244704–244715.
17. Glass CW, Oganov AR, Hansen N (2006) USPEX—evolutionary crystal structure prediction. *Comput Phys Commun* 175(11–12):713–720.
18. Dean MPM, et al. (2010) Neutron scattering study of the high-energy graphitic phonons in superconducting CaC<sub>6</sub>. *Phys Rev B* 82(1):014533.
19. Karen P, Kjekshus A, Huang Q, Karen VL (1999) The crystal structure of magnesium dicarbide. *J Alloy Comp* 282(1–2):72–75.
20. Palenzona A, Pani M (2004) The phase diagram of the Sr–Si system. *J Alloy Comp* 373(1–2):214–219.
21. Csányi G, Littlewood PB, Nevidomskyy AH, Pickard CJ, Simons BD (2005) The role of the interlayer state in the electronic structure of superconducting graphite intercalated compounds. *Nat Phys* 1(1):42–45.
22. Upton MH, et al. (2010) Phonons and superconductivity in YbC<sub>6</sub> and related compounds. *Phys Rev B* 82(13):134515.
23. Walters AC, et al. (2011) Comparative study of the phonons in nonsuperconducting BaC<sub>6</sub> and superconducting CaC<sub>6</sub> using inelastic x-ray scattering. *Phys Rev B* 84(1): 014511.
24. Rey N, et al. (2008) High-pressure behavior of CsC<sub>8</sub> graphite intercalation compound: Lattice structures and phase-transition mechanism. *Phys Rev B* 77(12):125433.
25. Nagel U, et al. (2008) Far-infrared signature of the superconducting gap in intercalated graphite CaC<sub>6</sub>. *Phys Rev B* 78(4):041404.
26. Weller TE, Ellerby M, Saxena SS, Smith RP, Skipper NT (2005) Superconductivity in the intercalated graphite compounds C<sub>6</sub>Yb and C<sub>6</sub>Ca. *Nat Phys* 1:39–41.
27. Emery N, et al. (2005) Superconductivity of bulk CaC<sub>6</sub>. *Phys Rev Lett* 95(8):087003.
28. Kim JS, Boeri L, O'Brien JR, Razavi FS, Kremer RK (2007) Superconductivity in heavy alkaline-Earth intercalated graphites. *Phys Rev Lett* 99(2):027001–027004.
29. Grüneis A, et al. (2009) Electronic structure and electron-phonon coupling of doped graphene layers in KC<sub>8</sub>. *Phys Rev B* 79(20):205106.
30. Zaleski-Ejgierd P, Hakala M, Pykkö P (2007) Comparison of chain versus sheet crystal structures for the cyanides MCN (M=Cu–Au) and dicarbides MC<sub>2</sub> (M=Be–Ba, Zn–Hg). *Phys Rev B* 76(9):094104.
31. Allen PB, Dynes RC (1975) Transition temperature of strong-coupled superconductors reanalyzed. *Phys Rev B* 12(3):905–922.
32. Profeta G, Calandra M, Mauri F (2012) Phonon-mediated superconductivity in graphene by lithium deposition. *Nat Phys* 8(2):131–134.
33. Kresse G, Furthmüller J (1996) Efficiency of *ab-initio* total energy calculations for metals and semiconductors using a plane-wave basis set. *Comput Mater Sci* 6(1): 15–50.
34. Blöchl PE (1994) Projector augmented-wave method. *Phys Rev B Condens Matter* 50(24):17953–17979.
35. Kresse G, Joubert D (1999) From ultrasoft pseudopotentials to the projector augmented-wave method. *Phys Rev B* 59(3):1758–1775.
36. Perdew JP, Burke K, Ernzerhof M (1996) Generalized gradient approximation made simple. *Phys Rev Lett* 77(18):3865–3868.
37. Giannozzi P, et al. (2009) QUANTUM ESPRESSO: A modular and open-source software project for quantum simulations of materials. *J Phys Condens Matter* 21(39):395502.
38. Vanderbilt D (1990) Soft self-consistent pseudopotentials in a generalized eigenvalue formalism. *Phys Rev B Condens Matter* 41(11):7892–7895.